FISEVIER

Contents lists available at ScienceDirect

### **Applied Surface Science Advances**

journal homepage: www.sciencedirect.com/journal/applied-surface-science-advances





## Facile synthesis of Co-Cu metal organic framework as efficient non-noble bifunctional electrocatalysts for overall water splitting

Ilaiyaraja Periyaiah <sup>a,1</sup>, M. Praveen Kumar <sup>b,\*\*</sup>, Natesan Kumaresan <sup>c</sup>, R.V. Mangalaraja <sup>b,d,\*\*</sup>, Francisco V. Herrera Diaz <sup>e</sup>, Saeed Farhang Sahlevani <sup>b,f</sup>, S. Sasikala <sup>g</sup>, G. Murugadoss <sup>h</sup>, Ilaiyaraja Perumal <sup>a,\*</sup>, Moorthy Sasikumar <sup>i,\*</sup>

- <sup>a</sup> Department of Chemistry, Vellore Institute of Technology, Vandalur, Kelambakkam Road, Chennai, Tamil Nadu 600127, India
- <sup>b</sup> Faculty of Engineering and Sciences, Universidad Adolfo Ibáñez, Diagonal las Torres 2640, Peñalolén, Santiago, Chile
- c Department of Physics, SSN Research Centre, Sri Sivasubramaniya Nadar College of Engineering, Chennai, Tamil Nadu 603110, India
- d Department of Mechanical Engineering, Faculty of Engineering, Karpagam Academy of Higher Education, Coimbatore, Tamil Nadu 641 021, India
- <sup>e</sup> Department Chemistry of Materials, Faculty of Chemistry and Biology, Universidad de Santiago, Santiago, Chile
- f Faculty of Engineering and Architecture, University of Arturo Prat, Iquique, Chile
- g Sainergy Fuel Cell, Perungudi Industrial Estate, Perungudi, Chennai, Tamilnadu 600 096, India
- <sup>h</sup> Centre for Nanoscience and Nanotechnology, Sathyabama Institute of Science and Technology, Chennai 600119, India
- <sup>i</sup> Dapartment of Physics, Bishop Heber College (Affiliated to Bharathidasan University), Tiruchirappalli, Tamilnadu 620 017, India

#### ARTICLE INFO

# Keywords: Cu MOF Co MOF Cu-Co MOF Chemical precipitation technique Bifunctional electrocatalysts OER HER Water splitting

#### ABSTRACT

The rapid development of superior, highly stable, alkaline-medium-compatible, and nonprecious earth-abundant bifunctional electrocatalysts has garnered significant research interest. This interest aims to replace the costliest noble metals (Pt, Ir/IrO<sub>2</sub>, and Ru/RuO<sub>2</sub>) in renewable and green energy technologies for overall water splitting. However, there are still important limitations, such as lower stability and higher energy consumption. In this work, we report the synthesis of Cu-Co metal-organic frameworks (MOFs) as a bifunctional electrocatalyst using a simple chemical precipitation technique. Especially, when 11.5 mM of Co is combined with Cu MOF, it exhibits excellent bifunctional activity for overall water splitting with a lower overpotential of 0.21 V (OER) and -0.71 V (HER) at a current density of 10 mA cm<sup>-2</sup>, which exhibits nearly several times more enhancement than that of pristine Cu and Co MOFs in a 1 M KOH electrolyte solution. The Tafel slope value of 130 mV/dec and the lower charge transfer resistance, along with relatively high stability for up to 12 h at the onset potential of OER and HER, are observed for the 11.5 mM Cu-Co MOF electrocatalyst. The present results open an alternative pathway for developing a novel design of highly efficient and scalable bifunctional electrocatalysts for overall water splitting.

#### 1. Introduction

A thriving global issue in the twenty-first century is mainly towards energy consumption, severe environmental pollution, and depletion of fossil fuels. Renewable energy technologies are focusing on green energy science [1]. In this light, hydrogen has been viewed as a promising alternative green energy source to displace fossil fuels because it is a clean and sustainable renewable energy source [1–4]. Accordingly, several strategies, including steam reforming [5], coal gasification [6],

biomass pyrolysis [7], and electrochemical water splitting [8,9], are extensively utilized for hydrogen generation. Among them, electrochemical water splitting seems to be a promising technology for producing pure hydrogen with zero emission of carbon [8,9]. The oxygen evolution reaction (OER) (at the anode) and hydrogen evolution reaction (HER) (at the cathode) are two half-reactions of water splitting, in which the hydrogen generation process has been implicated. However, the higher overpotential of OER and HER processes hinders their widespread applications [9–13]. Therefore, there is an emerging need

<sup>\*</sup> Corresponding authors.

<sup>\*\*</sup> Corresponding authors at: Faculty of Engineering and Sciences, Universidad Adolfo Ibáñez, Diagonal las Torres 2640, Peñalolén, Santiago, Chile.

E-mail addresses: praveenkumarmurugesan280589@gmail.com (M.P. Kumar), mangal@uai.cl (R.V. Mangalaraja), ilaiyaraja.perumal@vit.ac.in (I. Perumal), 84sasikumar@gmail.com (M. Sasikumar).

<sup>&</sup>lt;sup>1</sup> These authors contributed equally to this work.

for the design and development of highly active bifunctional electrocatalysts to minimize the overpotential during the OER and HER processes.

Platinum (Pt) serves as a benchmark catalyst for the hydrogen evolution reaction (HER) owing to its high activity and stability in an acidic medium [14]. Nevertheless, its inherent drawbacks, such as high cost and scarcity, necessitate the search for alternative catalysts. Moreover, platinum (Pt) is unsuitable for high oxygen evolution reaction (OER) voltages because its surface can be covered with an oxide, resulting in low electric or ionic conductivity. In contrast, Ir/IrO2 or Ru/RuO2 emerges as highly desirable nanomaterials for OER electrocatalysts [15]. However, these noble metals have unlikely garnered sufficient attention in the development of the oxygen evolution reaction (OER) due to their high price, limited supply, and poor stability in alkaline electrolyte media. Notably, the pH ranges of anode and cathode electrocatalysts differ, posing a severe challenge in integrating the two electrode reactions for large-scale electrolyzer applications [16,17].

Therefore, the advancement of materials science remains essential to replace those noble metals. New electrode materials are highly expected to serve as bifunctional electrocatalysts, performing effectively under various critical conditions and facilitating technology-level production. Accordingly, the focus has primarily been on D-block elements, such as metal sulphides [17-22], selenides [23,24], phosphides [25-28], nitrides [29-31], carbides [32,33], oxides [34-36], carbon with metals [37,38] and metal alloys [39–45], representing cost-effective substitutes for noble metals. Unfortunately, many electrocatalysts based on these materials exhibit minimal active sites, poor electrical conductivity, insufficient electrical contact with the electrolyte, and instability under operating conditions. Consequently, neither chemical exfoliation nor functionalization by compounds yields a high surface area. Nowadays, metal organic frameworks (MOFs) are of essential interest due to their exclusive structural advantages like porous nature, large specific surface area with tunable pores, changeful cavities, magnetizing optical, electrical, physiochemical properties along with adaptable chemistry [46-49], all of which make it the focus of research and development of MOFS as a bifunctional electrocatalysts for OER and HER reactions such as Ni-Co [50], Co-Fe [51], Ni-Fe [50], Cu-Fe [52], Cu-BTC [53], Cu-Co [46], etc. For instance, Peng et al., prepared a multifunctional book-like Cu-Co MOF using a one-step solvothermal method and it proved to be an efficient and highly stable electrocatalyst for OER in an alkaline medium [54]. As well, H. Lee et al. synthesized a bimetallic Co/Cu-embedded N-doped carbon structure using the pyrolysis process. This structure was successfully examined as a trifunctional electrocatalyst for oxygen reduction reaction (ORR), oxygen evolution reaction (OER), and hydrogen evolution reaction (HER) in an alkaline medium [55]. Undoubtedly, Cu and Co-based MOFs have been the primary focus as bifunctional electrocatalysts for overall water splitting applications in an alkaline medium due to their impressive properties, including high-volume abundance, outstanding redox characteristics, and ease of development.

These kinds of MOFs nanocomposites are prepared via a variety of processes, including hydrothermal [54], thermal treatment [56], chemical precipitation [56,57], solvothermal [55], and pulsed laser [58,59] methods, among others. Generally, many research works utilize the solvothermal method to prepare MOFs. In our case, we employed a simple chemical precipitation approach to produce Cu-Co MOF. This method allows us to control the structure, morphology, phase orientation, and temperature by adjusting various parameters.

Here, we developed the Cu-Co MOF via a simple chemical precipitation route as a bifunctional electrocatalyst using  $\rm H_2BDC$  as an organic linker. The  $\rm H_2BDC$  organic linker effectively supports the maintenance of surface morphology, specific surface area, and enhances charge transfer between the two metals and electrochemical active sites in the Cu-Co MOF. Furthermore, the Cu activity increased with the Co ratio (7.5, 9.5, 11.5, and 13.5 mM) for overall water splitting. The optimal concentration of 11.5 mM Co-functionalized Cu MOF exhibits excellent

activity for the oxygen evolution reaction (OER) with an onset potential of 1.44 V @ 10 mA cm $^{-2}$  and the hydrogen evolution reaction (HER) with overpotentials of 0.21 V and -0.71 V at a current density of 10 mA cm $^{-2}$ , respectively. This is in comparison to Ni plate (0.17 V), and it demonstrates good stability for 12 h in a 1 M KOH electrolyte solution. The overpotential is lower than that of currently reported nanomaterials, such as other MOFs, Ni-Fe LDH, Ni-Co alloy, and Fe-Cu nanocomposite. In addition, we conducted a full-cell water electrolyzer using Cu-Co MOF (11.5 mM) as both the anode and cathode in a 1 M KOH electrolyte solution. Moreover, the Cu-Co (11.5 mM) MOF proves to be an excellent electrocatalyst, not only as a replacement for noble metals but also due to its cost-effectiveness in developing water electrolyzer technology.

#### 2. Experimental section

#### 2.1. Materials

All chemical substances are of analytical grade (AR) and are used without further purification for the synthesis of MOFs. The  $CuSO_4 \cdot 5H_2O$ ,  $CO(NO_3)_2 \cdot 6H_2O$ , NaOH and  $H_2BDC$  were purchased from Sigma Aldrich.

#### 2.2. Preparation of Cu/Co-MOF, Cu-MOF, Co-MOF

A simple chemical precipitation method was employed to synthesize Cu-Co MOFs with different molarities.  $CuSO_4\cdot 5H_2O$  served as the copper oxide precursor, and varying amounts of  $CO(NO_3)_2\cdot 6H_2O$  were used for composite preparation. In a typical procedure,  $H_2BDC$  (12 mM, 0.0996 g) and NaOH (25 mM, 0.0499 g) were dissolved in 100 mL of deionized water with constant stirring for 30 min at room temperature. Subsequently, a 50 mL aqueous solution containing  $CuSO_4\cdot 5H_2O$  (7.5 mM, 0.0187 g) and  $CO(NO_3)_2\cdot 6H_2O$  (7.5 mM, 0.0218 g) was added dropwise to the above solution under vigorous stirring. After stirring for 5 h at room temperature, the resulting blue precipitate was isolated by filtration and thoroughly washed with water. Finally, the precipitate sample was subjected to a temperature of 70 °C for 24 h under vacuum conditions. For a comparison, Cu-MOF and Co-MOF were synthesized by treating 7.5 mM CuSO<sub>4</sub>·5H<sub>2</sub>O and 7.5 mM CO (NO<sub>3</sub>)<sub>2</sub>·6H<sub>2</sub>O, respectively, with 12 mM H<sub>2</sub>BDC.

#### 2.3. Physico-chemical characterization

The structural and crystallinity information of the Cu, Co, and Cu-Co MOFs network was determined using the advanced X-ray diffractometer (XRD, Bruker D8 with Cu-K $\alpha$  ( $\lambda = 1.5405$ ) radiation). Raman spectroscopy provided insights into the vibrational modes of molecules, and spectra were collected using the Renishaw (UK) InVia Raman microscope with a 632.8 nm wavelength incident laser light. The Fourier transform-infrared (FT-IR) spectrometer was used to detect the presence of functional groups in the prepared Cu-Co MOFs (TENSOR27; BRUKER OPTIK GMBH, Germany). Scanning electron microscopy (SEM, Model Hitachi S-4500) was employed to examine the morphology of the produced samples. The powder sample was thoroughly mixed with ethanol before being drop-cast onto a gold-coated copper grid and then dried. The elemental composition of the Cu-Co MOF was examined using the PHI 5000 VersaProbe ULVAC apparatus and X-ray photoelectron spectroscopy (XPS). Electrochemical analysis was conducted at room temperature utilizing an electrochemical workstation (SP-150, Biologic Science Instruments, France). A standard three-electrode setup with platinum as the counter electrode, Hg/HgO as the reference electrode, and Cu-Co MOF as the working electrode was used.

#### 3. Result and discussion

#### 3.1. Structural investigation through X-ray diffraction patterns

The powder X-ray diffraction (XRD) patterns were recorded to determine the crystal phase and structure of the sample. The XRD characterization is very good tool to investigate the formation of MOFs in the prepared samples. Fig. 1 shows the XRD patterns for Cu MOF, Co MOF and Cu-Co MOF. Fig. 1a represents the XRD pattern of Cu MOF, in which characteristic peaks appeared at  $2\theta = 6.5^{\circ}$ ,  $9.5^{\circ}$ ,  $12.9^{\circ}$ ,  $13.5^{\circ}$ , 14.9°, 16.2°, 17.5°, 19.8°, 21.4°, 24.5°, 26.2° 29.3°, 35.3° and 39.5° correspond to the (200), (220), (222), (400), (420), (422), (511), (440), (442), (551), (731), (751), (773) and (882) crystal planes respectively and are consistent with previous reported literature (Cambridge crystallographic information data with deposit number of 112,954). A less intensity peak at 16.5 is noticeable in the Cu-MOF sample, which is related to the presence of some organic residue on Cu-MOF [60,61]. Further, Fig. 1b shows sharp diffraction peaks at 20 of 9.18°, 15.8°. 17.5°, 29.5° correspond to (020) (120), (112), and (105) lattice planes of Co<sub>2</sub> MOF respectively. The diffraction peaks positions of Co<sub>2</sub> MOF are in good agreement with the simulation based on Co-MOF single-crystal XRD data (Cambridge Crystallographic Data centre - 905,134) [62]. Further, the Cu-Co MOF reveals the diffraction peaks at 9.18°, 15.8° and 18.5° are related to the (020), (120) and (112) plane of Co<sub>2</sub> MOF respectively. Further, the peak observed at 17.2°, 24.6°, 27.61° and  $28.3^{\circ}$  are related to the (511), (551), (731) and (751) of Cu MOF respectively (Fig. 1c). In the present work, it is clearly confirmed the presence of Cu and Co with the network contact of some organic residue in Cu-Co MOF. The two metal phases are presented in the Cu-Co MOF. Furthermore, compared with the Cu and Co MOFs, the diffraction peaks of Cu-Co MOF sample are shifted to higher angles (Fig. 1c) [63].

#### 3.2. Raman spectra analysis for Cu, Co and Cu-Co MOFs

The Raman spectra were obtained to investigate the Cu, Co, and Cu-Co MOFs, as shown in Fig. 2. Fig. 2a displays the Raman spectrum of Cu MOF, revealing peaks at 284.3, 324.1, and 363.8 cm $^{-1}$ , corresponding to the formation of CuO. More specifically, the wavenumber at 284.3 cm $^{-1}$  attributes to Ag, while the peaks at 357.4 and 363.8 cm $^{-1}$  ascribe to Bg modes for Cu MOF [64]. The Co MOF exhibits peaks at 431.8 (Co-O), 500.8, and 607.8 cm $^{-1}$ , as depicted in Fig. 2b. The remaining two peaks are indicative of the spinel structure of Co<sub>3</sub>O<sub>4</sub> nanorods. Specifically, the Raman peaks of the Co MOF correspond to the Eg, F2g, and A1g modes of Co<sub>3</sub>O<sub>4</sub> [65]. Additionally, the major Raman peaks of the Cu-Co MOF

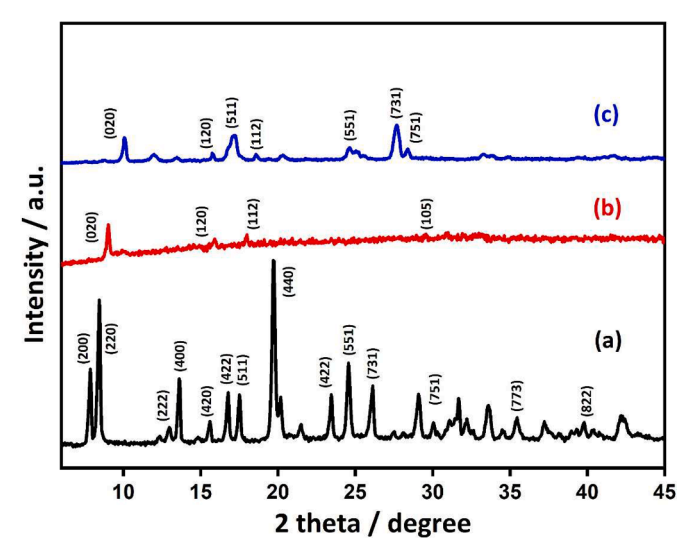


Fig. 1. The XRD patterns of (a) Cu, (b) Co and (c) Cu-Co MOFs.

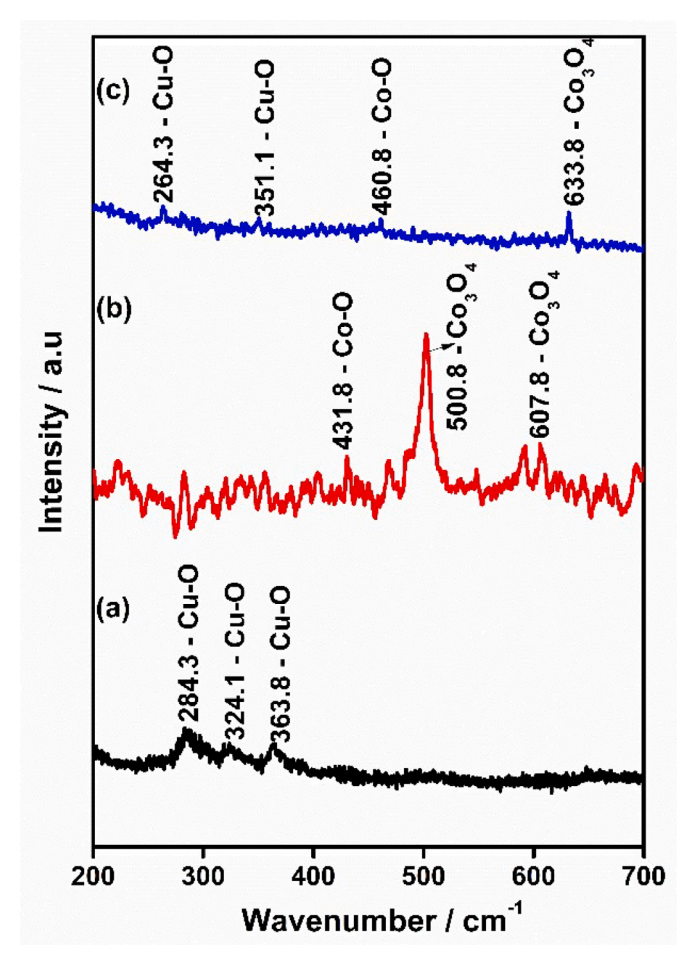


Fig. 2. The Raman spectra of (a) Cu (b) Co and Cu-Co MOFs.

are shown in Fig. 2c, with peaks observed at 264.6 and 351.1 cm $^{-1}$  corresponding to the modes of CuO, and peaks at 460.8 and 633.8 cm $^{-1}$  corresponding to the modes of Co $_3$ O $_4$ . It is noteworthy that the spectrum indicates the formation of CuO—Co $_3$ O $_4$  MOF [64.65].

#### 3.3. Functional groups analysis

The FT-IR vibrational spectra determine the presence of organic composites and the creation of new functional groups in the as-prepared

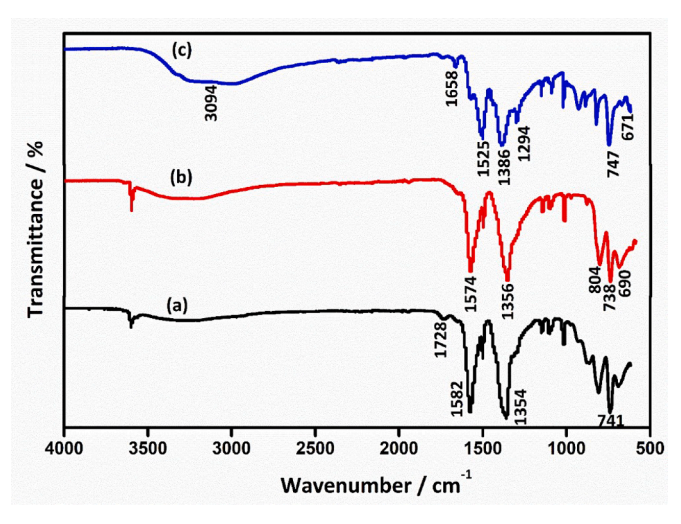


Fig. 3. FT-IR spectra of (a) Cu, (b) Co and (c) Cu-Co MOFs.

MOFs. Fig. 3 exhibits the FT-IR spectra of Cu, Co, and Cu-Co MOFs. In Fig. 3a, the FTIR spectrum of Cu MOF shows major peaks at 1728 and 1582 cm<sup>-1</sup>, corresponding to the asymmetric vibrations of the carboxylate groups of benzenetricarboxylate ligands, while 1354 and 741  ${\rm cm}^{-1}$ correspond to the symmetric vibrations of benzenetricarboxylate ligands and Cu-O-H, respectively [66]. The vibrational peaks of the Co MOF at 1574 and 1356 cm<sup>-1</sup> attribute to the stretching vibrations of C=O and C-O, respectively, as shown in Fig. 3b. Additionally, the absorption peaks at 804, 738, and 690 cm<sup>-1</sup>, correspond to the aromatic ring stretching C—H, flexural vibrations of Co-O-H, and stretching vibrations of para-aromatic C—H groups, respectively [60,67] (Fig. 3b). The broad peak at 3094 cm<sup>-1</sup> is uniquely present in the Cu-Co MOF, indicating the presence of absorbed water on the surface [60,67] (Fig. 3c). Moreover, two strong vibrational peaks at  $\sim$ 1658 and 1294 cm $^{-1}$  are attributed to the asymmetric and symmetric stretching vibrational modes of the synchronized (COO-) group, respectively. Fig. 3c displays absorption peaks at 1580 and 1360 cm<sup>-1</sup> are mainly attributed to the coordination of Cu<sup>2+</sup> and Co<sup>2+</sup> with hydroxyl groups, promoting the deprotonation of the Cu-Co MOF. Similarly, the  $\Delta \nu$  value of 220 cm<sup>-1</sup> between two vibrational bands is less than that observed in the spectra of a and b, indicating the synchronization of metal ions and hydroxyl oxygen in a bidentate bridge. Moreover, the two absorption peaks near 750 - 747 cm<sup>-1</sup> are ascribed as tensile and flexural vibrations of Cu-O-H and Co-O–H in the Cu-Co MOF. Finally, the overall investigation firmly confirms the successful synthesis of the MOF as an electrocatalyst. Additionally, the peak at 671 cm<sup>-1</sup> corresponds to the vibrational band of C—H [46]. The FT-IR characterization further confirms the presence of carboxylic groups as well as several oxidations in the Cu-Co MOF. These parameters are deemed more suitable to enhance the electrocatalytic activity in overall water splitting. Moreover, Fig. S1 shows the FT-IR spectrum for H<sub>2</sub>BDC.

#### 3.4. Investigation on surface morphology, elements and mapping

The surface morphology of Cu, Co and Cu-Co MOFs was characterized by FE-SEM. Fig. 4a shows the self-assembled columnar shaped with

around many dispersed nanoparticles of Cu MOF. Co MOF shows a nanosheet with size of 50 nm in Fig. 4b, while the Cu-Co MOF possesses the Cu MOF nanoparticles perfectly placed on the Co MOF sheets with the control size. Moreover, the combination of nanosheet and particles can create more surface area as well as more electroactive sites to favor the reactions of the overall water splitting. The FE-SEM image of Cu-Co MOF is proving significance of surface morphology in Fig. 4c. In addition, the EDAX spectra were caried out for Cu, Co and Cu-Co MOFs, as shown in Fig. 4d–f. The Fig. 4d exhibits Cu, O and C elements for Cu MOF, as well as Co, O and C elements were presented in Co MOF (Fig. 4e). Both spectra confirmation of single-phase MOFs. Moreover, The EDAX spectrum of Cu-Co MOF shows presence of Cu, Co, O and C elements, as shown in Fig. 4f, which is confirmation of formation of Cu and Co. Consequently, the percentage of all elements were observed for each Cu, Co and Cu-Co MOFs in Fig. 4g-i, respectively.

The elements mapping is the one of the good techniques to investigate the presence and quantify of elements for as prepared nanomaterials. The Fig. 5 shows the elementals mapping for Cu-Co MOF. Fig. 5a exhibits elementals mapping survey of Cu-Co MOF, where confirmed presence of all elements. Frequently, the Fig. 5b-e represents elementals mapping high resolution spectra for C, O, Cu and Co, respectively. From these results, we confirmed formation of Cu-Co MOF. Moreover, Fig. S8 shows the elements mapping for Cu and Co MOFs.

#### 3.5. Determination of elements and oxidation level

Fig. 6a represents the high resolution spectrum of Cu2p from Cu MOF. The deconvolution peaks are presented at 930.9, 933.8, 941, 943.6, 950.7 and 954 eV corresponding to Cu(I) and Cu(II) for Cu<sub>3/2</sub>, satellite peaks and Cu(I) and Cu(II) for Cu<sub>1/2</sub>, respectively. This result is confirmed the oxidation state of Cu. In Fig. 6b, the O1s major peaks were appeared at 531.1 eV for C—O-Cu, 531.8 eV for C=O and 532.8 eV for OH. The XPS study is concluded that Cu MOF was effectively prepared. The XPS high resolution spectra of Co MOF shown in Fig. 6c and d for Co2p and O1s. The deconvolution of Co2p were contained five major peaks. The peaks at 776.7 and 780.3 eV for Co2p<sub>3/2</sub> can be revealed to

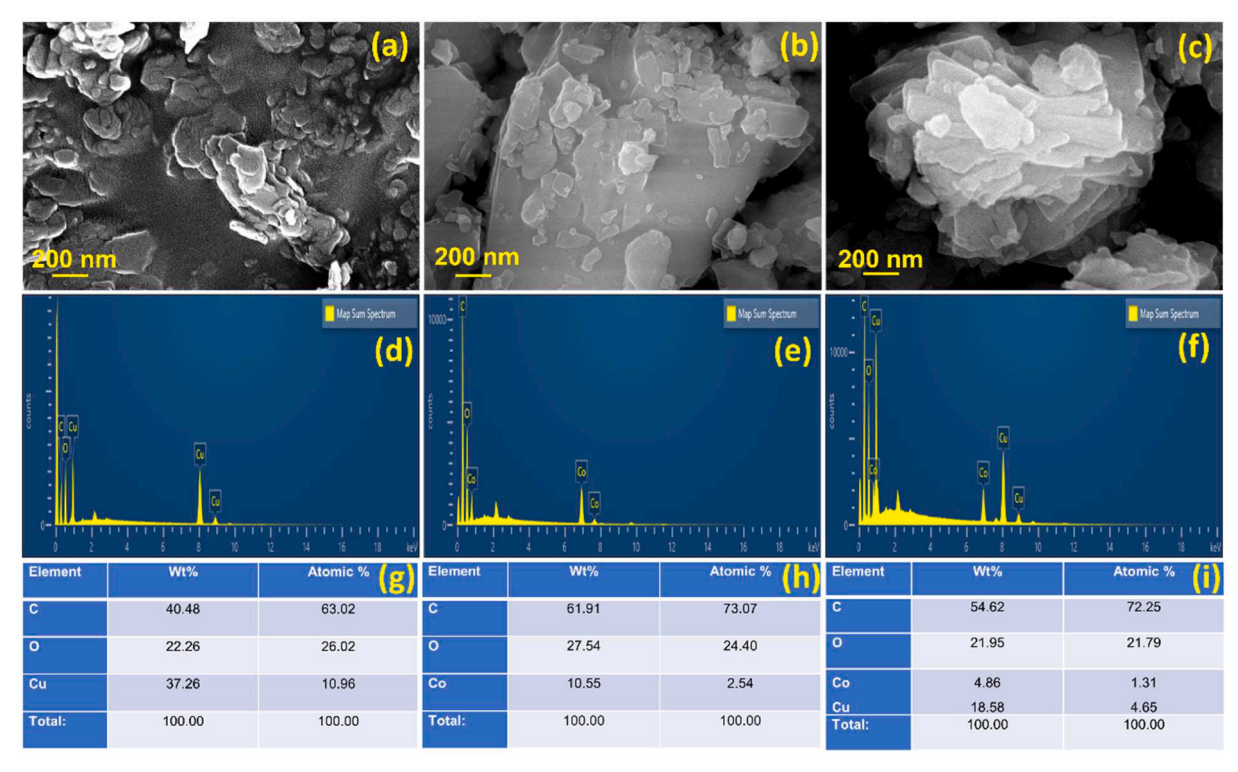


Fig. 4. The FE-SEM images of (a) Cu, (b) Co and (c) Cu-Co MOFs. (d-f) the EDAX spectra and (g-i) percentage of all elements for Cu, Co and Cu-Co MOFs.

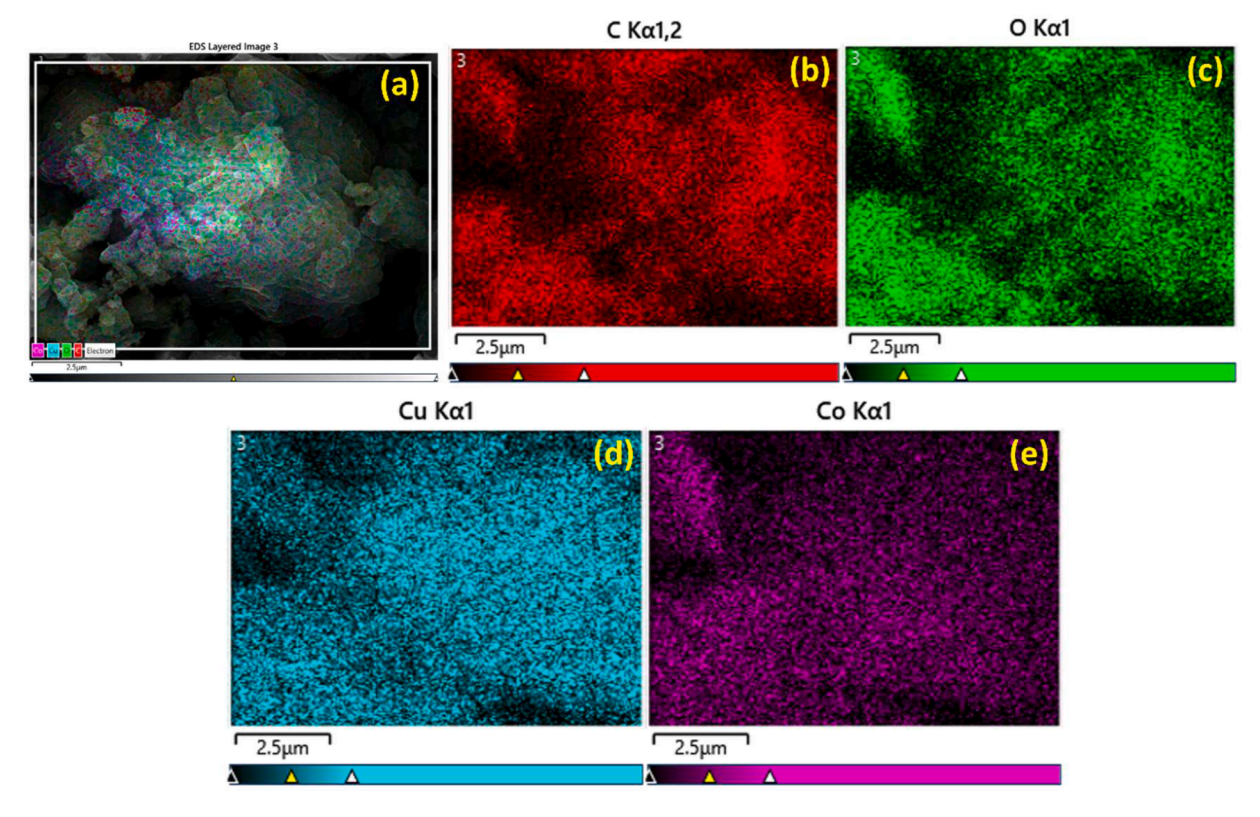


Fig. 5. The Elements mapping of (a) Cu-Co MOFs. (b-d) corresponding mapping for Cu, Co, O and C.

oxidation of Co(II) and Co(III), which is due to oxidation in air. The peak at 783 eV is attributed to satellite peak due to charge transfer shakeup. The two peaks at 796.5 and 800.7 eV for  $Co2p_{1/2}$  might be Co oxidized species. The O1s two major peaks were appeared at 531.1 and 532.2 eV for C—O-Co and C=O, respectively (Fig. 6d). From XPS investigation, the Co MOF was synthesised via simple chemical precipitation method.

The characterization of XPS was used to determine the chemical composition of the prepared MOF. The peaks of Cu, Co and O elements are clearly observed at 935, 785 and 527 eV from the XPS survey spectrum, as shown Fig. 7a. Fig. 7b shows the XPS high resolution spectrum of Cu 2p, which indicates the coexistence of Cu(I) and Cu(II) oxidation level on the catalyst surface. The Cu2p<sub>3/2</sub> XPS spectra are split into two major peaks at the binding energies of 929.6 and 928 eV corresponding to Cu(II) and Cu(I), respectively. While the Cu2p<sub>1/2</sub> XPS spectra can be fitted into two main peaks at 947.7 and 949.3 eV, attributed to Cu(I) and Cu(II) species, respectively [68]. In addition, the binding energy of 934.9, 939, 954 and 957.7 eV indicates the appearance of satellite peak, revealing the presence of Cu(II) species in Cu MOF [68]. Fig. 7c, the high-resolution XPS spectrum of Co2p shows two major peaks at 780.5 and 795.4 eV (Co $2p_{1/2}$ ). Subsequently, the two major peaks are deconvoluted into four peaks at 779.5, 780.6, 792.5 and 797.1 eV, revealing the co-existence of +2 and +3 oxidation states for Co ions [69]. In Fig. 7d, the XPS spectrum of O 1 s is deconvoluted into three peaks with binding energy of 526.3, 527 and 528.1 eV for lattice oxygen in an oxygen-deficient environment with  $O^{2-}$  vacancies, water adsorption on the surface of catalyst and a typical metal-oxygen bond, respectively [69,70]. The Cu-Co MOF exhibits various oxidation states, consistent with XPS result. Based on these findings, we conclude that the Cu-Co MOF nanomaterial is well-suited for overall water splitting, serving as a bifunctional electrocatalyst in an alkaline medium.

#### 3.6. Electrochemical analysis

#### 3.6.1. OER

For the analysis of electrocatalytic activity toward OER, we

employed a standard three-electrode system. The Cu-Co MOFs served as the working electrode, Pt wire as the counter electrode, and Hg/HgO as the reference electrode. The experiments were conducted in a 1.0 M KOH aqueous solution at a scan rate of 10 mV/s. Bare Cu, Co, and different ratios of Cu-Co MOFs were also tested in the same environment for comparison. Fig. 8a represents the linear sweep voltammetry (LSV) curves for bare Cu, Co, CuO-Co MOFs and bare Ni plate. Cu-Co MOF shows the excellent electrocatalytic activity for OER with the onsetpotential of 1.32 V (0.21 V overpotential (@10 mA cm<sup>-2</sup>). On the other hand, the onset potential of Cu-Co MOF is lower than that of bare Cu (1.48 V) and Co (1.40 V) MOFs, and comparable to that of a bare Ni plate (1.31 V). The results indicate that the incorporation of Co is effective in reducing the onset potential of Cu during OER. Hence, the inset of Fig. 8a provides an enlarged scale of the onset potential for bare Cu, Co, CuO-Co MOFs, and bare Ni plate. Furthermore, we conducted OER activity tests for different percentages of Co functionalization (7.5, 9.5, 11.5, and 13.5 mM) on the surface of Cu (Fig. S2a). The onset potentials for 7.5, 9.5, 11.5, and 13.5 mM are 1.36, 1.45, 1.32, and 1.46 V, respectively. As expected, the Cu-Co MOF (with a Co ratio of 11.5 mM) exhibits superior OER activity compared to others. The low amount of Co is insufficient to enhance the OER of Cu MOF. However, upon further increasing the Co functionality percentage to 13.5 mM, OER activity decreases. This observation clearly indicates that the presence of Co considerably enhances the OER activity of Cu MOF. Tafel slope values are calculated from the potential versus log |i| in the linear region above the onset potential of OER, as shown in Fig. 8b. The Tafel slope value of 11.5 mM Cu-Co MOF exhibits the lowest 130 mV/dec. Moreover, the Cu (149 mV/dec) and Co MOFs (145 mV/dec) shows a highest Tafel slope value, comparable to bare Ni plate (64 mV/dec). The Tafel slope values of 147, 137 and 139 mV/dec obtained for 7.5, 9.5 and 13.5 mM, respectively, which are higher than 11.5 mM (Fig. S2b). A lesser Tafel slope value of 11.5 mM Cu-Co MOF is kinetically favors an electrochemical OER reaction. Moreover, we have plotted the comparison of onsetpotential, @10 mA onsetpotential and overpotential for all samples, as shown Fig. 8c. The comparison plot (onsetpotential, @10 mA

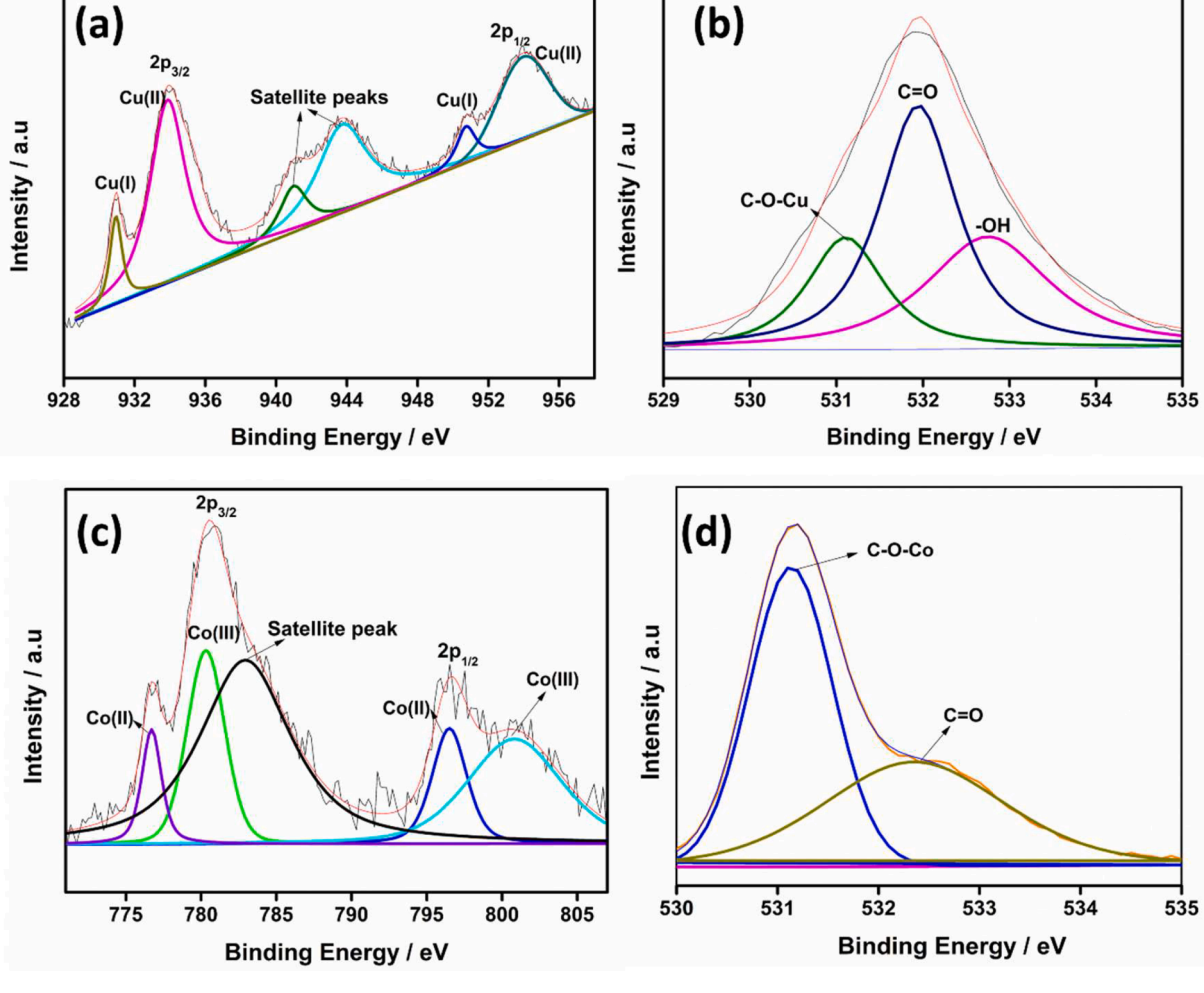


Fig. 6. XPS high resolution of (a) Cu2p, (b) O1s for Cu MOF, (c) Co2p and (d) O1s for Co MOF.

onsetpotential and @10 mA overpotential) clearly shows the 11.5 mM Cu-Co MOF is highly active compared to other samples and comparable to bare Ni plate. The Kinetic current is also one of the key roles to identify the catalytic activity of electrocatalyst. the comparison bar chart of kinetic current for Cu, Co, Cu-Co MOFs and bare Ni plate in Fig. 8d. Cu-Co MOF exhibits higher kinetic current compared to bare Cu and Co MOFs, comparable to bare Ni Plate. Consequently, the comparison bar chat of 11.5 mM Cu-Co MOF plotted with 7.5, 9.5 and 13.5 mM, as shown in Fig. S2c. Fig. 8e shows the chronoamperometry study of 11.5 mM Cu-Co MOF materials, which is higher stability for 12 hrs. Hence, the Cu-Co MOF (11.5 mM) shows low onsetpotential of 1.44 V compared to Pt/C, as shown in Fig. S5. Moreover, we calculated the electrochemical surface-active sites (ESCA) using OER cyclic voltametric technique for Cu, Co and Cu-Co MOFs (Fig. S6).

#### 3.6.2. HER

To evaluate the HER process over the samples, we used the same OER conditions as mentioned above. In Fig. 9a, the LSV curve for Cu, Co, Cu-Co MOFs, and bare Ni plate is presented. An onset potential of -0.59 V was obtained for Cu-Co MOF (11.5 mM), which is lower than that of bare Cu (-0.99 V) and Co (-0.71 V) MOFs, but comparable to the onset potential of the bare Ni plate (-0.40 V). Additionally, the lower onset potential of Cu-Co MOF (11.5 mM) is compared with other concentrations, such as Cu-Co MOF (7.5 mM) (-0.70 V), Cu-Co MOF (9.5 mM) (-0.67 V), and Cu-Co MOF (13.5 mM) (-0.65 V) (as shown in Fig. S3a). Furthermore, the Tafel slope values of these catalysts were plotted from LSV data to estimate the aspects of the reaction kinetics. Fig. 9b shows

the Tafel slope values of Cu, Co, Cu-Co MOF (11.5 mM), and bare Ni plate, which are 347 mV/dec, 93 mV/dec, 87 mV/dec, and 63 mV/dec, respectively. Moreover, the Tafel value of Cu-Co MOF (11.5 mM) is compared with Cu-Co MOF (7.5 mM, -114 mV/dec), Cu-Co MOF (9.5 mM, -99 mV/dec), and Cu-Co MOF (13.5 mM, -95 mV/dec), as shown in Fig. S3b. The Cu-Co MOF (11.5 mM) exhibits a lower Tafel value compared to other MOFs, highlighting its suitability for the HER process. Fig. 9c represents the comparison plot (onset potential, @10 mA onset potential, and @10 mA overpotential) of all the above samples. From this plot, Cu-Co MOF (11.5 mM) exhibits lower values compared to other catalysts, which is more favorable for HER. Hence, the comparison bar chart of kinetic current for Cu, Co, Cu-Co MOFs (11.5 mM), and bare Ni plate is shown in Fig. 9d. Cu-Co MOF (11.5 mM) exhibits a higher kinetic current compared to Cu and Co MOFs for the HER process. In Fig. S3c, the comparison bar chart is plotted for onset potential, @10 mA onset potential, and @10 mA overpotential for Cu-Co MOF (7.5 mM), Cu-Co MOF (9.5 mM), Cu-Co MOF (11.5 mM), and Cu-Co MOF (13.5 mM). Moreover, Cu-Co MOF (11.5 mM) shows good stability for 12 h in a 1 M KOH electrolyte (Fig. 9e). Hence, Cu-Co MOF (11.5 mM) exhibits a higher current density of 140 mA cm-2 compared to Pt/C, as shown in Fig. S5. Moreover, we calculate the electrochemical surface-active sites (ESCA) using HER cyclic voltammetry for Cu, Co, and Cu-Co MOFs (Fig. S7). According to the electrochemical results, Cu-Co MOF (11.5 mM) could be utilized as a bifunctional electrocatalyst for overall water splitting in an alkaline medium, making it very suitable for replacing noble metals in large-scale applications.

Cu-Co MOF (11.5 mM) demonstrates excellent bifunctional activity

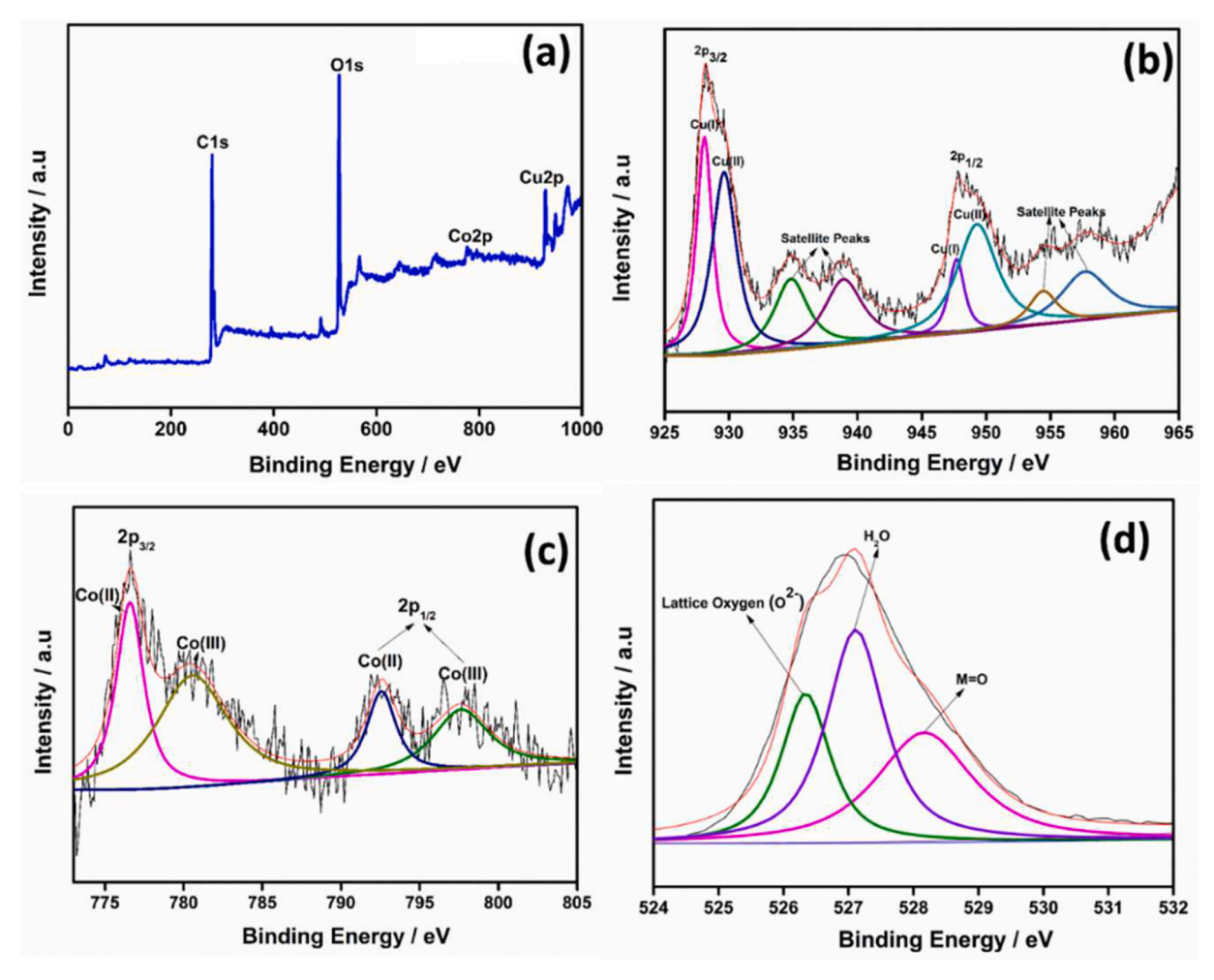


Fig. 7. XPS survey spectra of (a) Cu-Co MOF. (b) Cu2p, (c) Co2p and O1s XPS high resolution of Cu-Co MOF.

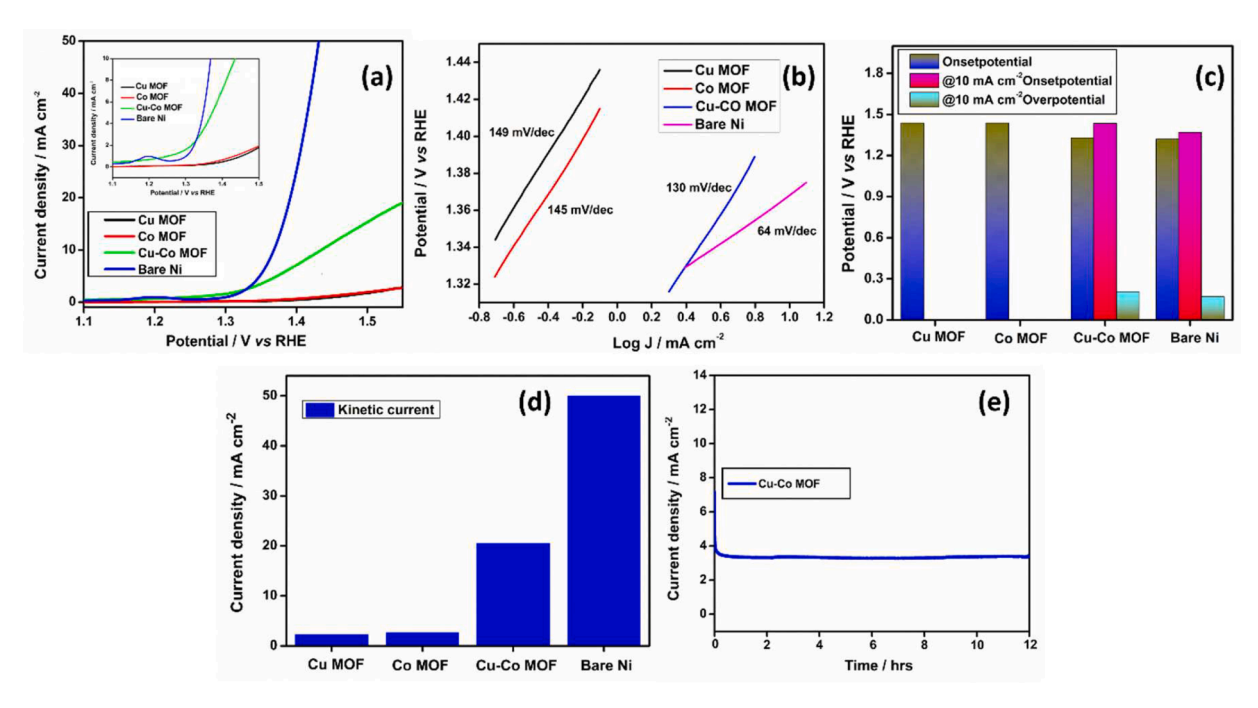


Fig. 8. (a) OER studies (LSV) and enlarge the onsetpotential (insert) (b) Tafel slope values and (c) comparison bar chart (onsetpotential, @10 mA onsetpotential and overpotential), (d) comparison bar chart (Kinetic current) of Cu MOF, Co MOF, Cu-Co MOF and Ni plate. (e) Stability tested using chronoamperometry technique for Cu-Co MOF.

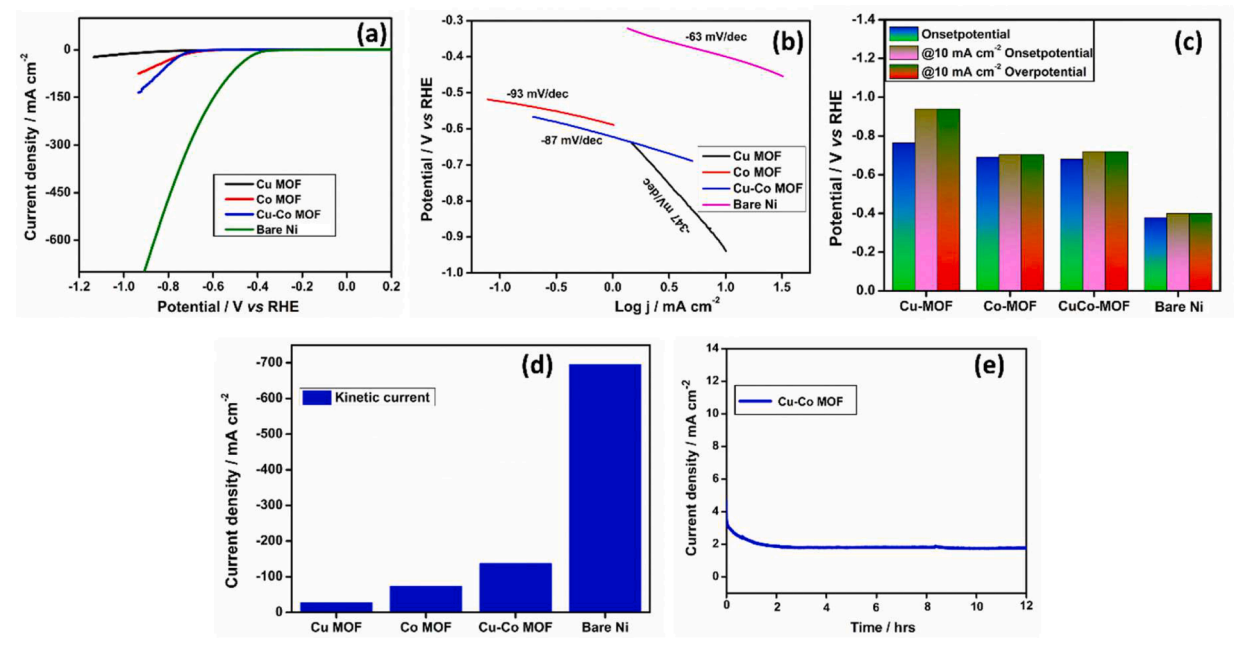


Fig. 9. (a) HER studies (LSV) (b) Tafel slope values and (c) comparison bar chart and (d) comparison bar chart (Kinetic current) (onsetpotential, @10 mA onsetpotential and overpotential) of Cu MOF, Co MOF, Cu-Co MOF and bare Ni plate. (e) Stability tested using chronoamperometry technique for Cu-Co MOF.

for OER and HER in an alkaline medium. We conducted a full cell water electrolyzer using Cu-Co MOF electrocatalyst (11.5 mM) as anode and cathode materials in a 1 M KOH electrolyte solution. The area of the water electrolyzer cell is 25 cm $^2$ . The electrocatalyst exhibits a current density of 11.9 A cm $^{-2}$  at 1.9 V, as shown in Fig. 10. The results of the full cell water electrolyzer confirm that Cu-Co MOF electrocatalyst is one of the best and most cost-effective catalysts for overall water splitting in an alkaline medium. Furthermore, Table S1 shows a comparison of the onset potential of Cu-Co MOF (11.5 mM) with other works.

#### 3.6.3. Electrochemical impedance spectroscopic

Electrochemical impedance spectroscopic (EIS) analysis was carried out to gain further insight into the high OER and HER activities of bare Cu, Co, and Cu-Co MOFs (11.5 mM) through Nyquist plots. The Nyquist plots of bare Cu, Co, and Cu-Co MOF (11.5 mM) were obtained under the same OER and HER conditions (versus Hg/HgO) in 1.0 M KOH, applying the frequency ranging from 10 Hz to 1 MHz with an AC amplitude of 5

mV (Fig. 11). The smallest semicircle value is observed with Cu-Co MOF (11.5 mM), indicating its good catalytic activity and quicker electron transport rate, leading to the smallest Tafel slope value, as shown in Fig. 11.

#### 4. Conclusion

In this work, we developed Cu-Co MOF through a self-assembling solvothermal method, acting as a bifunctional electrocatalyst for OER and HER in an alkaline medium. Moreover, the amount of Co was optimized to enhance the catalytic activity of Cu MOF by varying the concentration of CO(NO3)2·6H2O. The Cu-Co MOF (11.5 mM) exhibited high activity with overpotential of 0.21 V (OER) and -0.71 V (HER) at a current density of 10 mA cm-2, outperforming bare Cu, Co, and other concentration MOFs. The EIS study revealed a smaller diameter semicircle for Cu-Co MOF compared to bare Cu and Co, indicating lower charge transfer resistance for Cu-Co (11.5 mM) MOF. Furthermore, Cu-

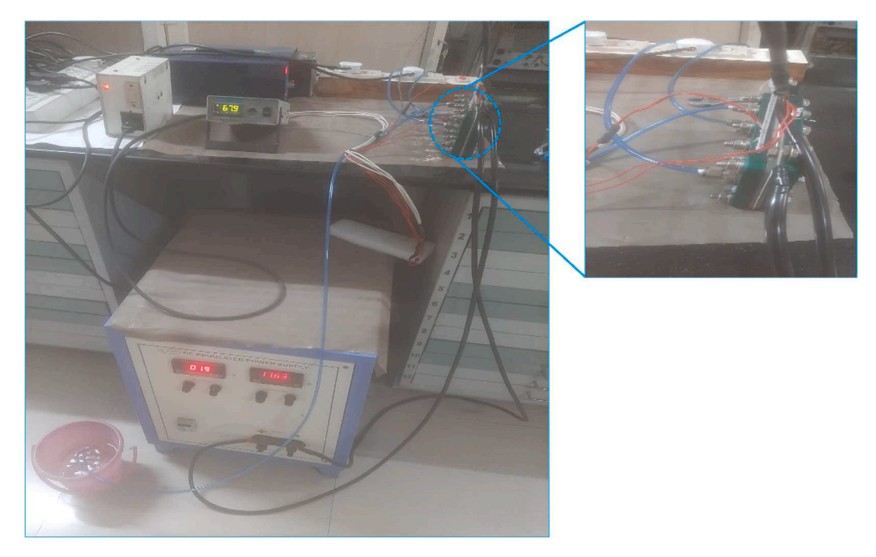


Fig 10. Cu-Co MOF is used as an anode and cathode in a full cell water electrolyzer.

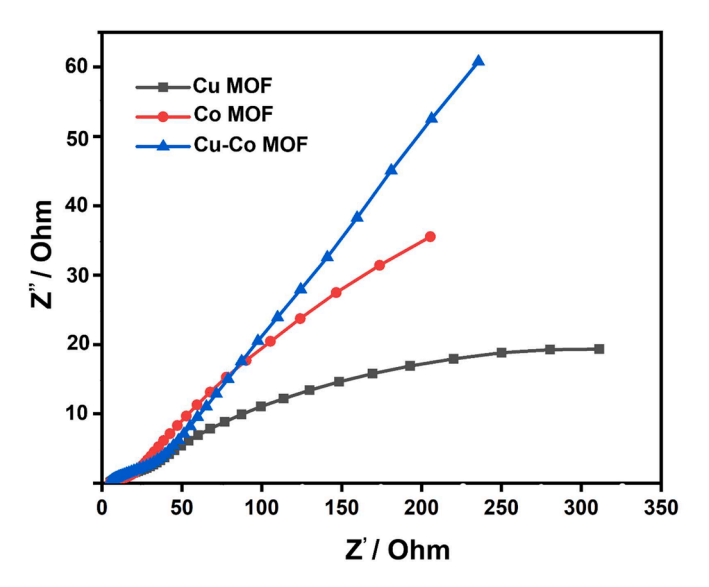


Fig. 11. EIS Nyquist plots of Cu, Co and Cu-Co MOFs.

Co (11.5 mM) MOF demonstrated stability for 12 h in a 1 M KOH solution. The developed catalyst offers bifunctionality, high activity, low cost, and stability for overall water splitting in an alkaline medium. This presents a new opportunity to replace noble metals towards enhancing OER and HER.

#### CRediT authorship contribution statement

Ilaiyaraja Periyaiah: Investigation. M. Praveen Kumar: Investigation, Methodology, Supervision, Visualization, Writing – original draft. Natesan Kumaresan: Visualization, Writing – review & editing. R.V. Mangalaraja: Supervision, Visualization, Writing – review & editing. Francisco V. Herrera Diaz: Visualization, Writing – review & editing. Saeed Farhang Sahlevani: Visualization. S. Sasikala: Visualization. G. Murugadoss: Visualization, Writing – review & editing. Ilaiyaraja Perumal: Visualization, Writing – review & editing. Moorthy Sasikumar: Investigation, Visualization, Writing – original draft, Writing – review & editing.

#### **Declaration of competing interest**

The authors declare that they have no known competing financial interests or personal relationships that could have appeared to influence the work reported in this paper.

#### Data availability

Data will be made available on request.

#### Acknowledgement

The authors Praveen Kumar and Mangalaraja would like to thank to the ANID-FONDECYT postdoctoral project No. 3220475, Government of Chile, Santiago, Chile for the financial support. Mooorthy Sasikumar would like to acknowledge the financial support (MRP/1006/2023) from the Bishop Heber College, Tiruchirappalli, Tamil Nadu, India.

#### Supplementary materials

Supplementary material associated with this article can be found, in the online version, at doi:10.1016/j.apsadv.2024.100593.

#### References

- D. Larcher, J.M. Tarascon, Towards greener and more sustainable batteries for electrical energy storage, Nat. Chem. 7 (2015) 19–29, https://doi.org/10.1038/ nchem.2085.
- [2] Z.W. She, J. Kibsgaard, C.F. Dickens, I. Chorkendorff, J.K. Nørskov, T.F. Jaramillo, Combining theory and experiment in electrocatalysis: insights into materials design, Science (2017) 355, https://doi.org/10.1126/science.aad4998 (1979).
- [3] G. Ye, Y. Gong, J. Lin, B. Li, Y. He, S.T. Pantelides, W. Zhou, R. Vajtai, P.M. Ajayan, Defects engineered monolayer MoS<sub>2</sub> for improved hydrogen evolution reaction, Nano Lett. 16 (2016) 1097–1103, https://doi.org/10.1021/acs.nanolett.5b04331.
- [4] L. Liu, Z. Jiang, L. Fang, H. Xu, H. Zhang, X. Gu, Y. Wang, Probing the crystal plane effect of Co<sub>3</sub>O<sub>4</sub> for enhanced electrocatalytic performance toward efficient overall water splitting, ACS Appl. Mater. Interfaces 9 (2017) 27736–27744, https://doi. org/10.1021/acsami.7b07793.
- [5] E.C. Vagia, A.A. Lemonidou, Hydrogen production via steam reforming of bio-oil components over calcium aluminate supported nickel and noble metal catalysts, Appl. Catal. A Gen. 351 (2008) 111–121, https://doi.org/10.1016/j. apcata.2008.09.007.
- [6] Y. Sun, J. Nakano, L. Liu, X. Wang, Z. Zhang, Achieving waste to energy through sewage sludge gasification using hot slags: syngas production, Sci. Rep. 5 (2015), https://doi.org/10.1038/srep11436.
- [7] A. Melis, T. Happe, Hydrogen production. Green algae as a source of energy, Plant Physiol. 127 (2001) 740–748, https://doi.org/10.1104/pp.010498.
- [8] M. Buscema, J.O. Island, D.J. Groenendijk, S.I. Blanter, G.A. Steele, H.S.J. Van Der Zant, A. Castellanos-Gomez, Photocurrent generation with two-dimensional van der Waals semiconductors, Chem. Soc. Rev. 44 (2015) 3691–3718, https://doi.org/ 10.1039/c5cs0106d
- [9] C.S. Saraj, S.C. Singh, G. Verma, A. Alquliah, W. Li, C. Guo, Rapid fabrication of CuMoO<sub>4</sub> nanocomposites via electric field assisted pulsed-laser ablation in liquids for electrochemical hydrogen generation, Appl. Surf. Sci. Adv. 13 (2023) 100358, https://doi.org/10.1016/j.apsadv.2022.100358.
- [10] A. Raza, A.A. Rafi, J.Z. Hassan, A. Rafiq, G. Li, Rational design of 2D heterostructured photo- & electro-catalysts for hydrogen evolution reaction: a review, Appl. Surf. Sci. Adv. 15 (2023) 100402, https://doi.org/10.1016/j. apsadv.2023.100402.
- [11] A. Vazhayil, L. Vazhayal, J. Thomas, S. Ashok C, N. Thomas, A comprehensive review on the recent developments in transition metal-based electrocatalysts for oxygen evolution reaction, Appl. Surf. Sci. Adv. 6 (2021) 100184, https://doi.org/ 10.1016/j.apsadv.2021.100184.
- [12] A. Gowrisankar, A.L. Sherryn, T. Selvaraju, In situ integrated 2D reduced graphene oxide nanosheets with MoSSe for hydrogen evolution reaction and supercapacitor application, Appl. Surf. Sci. Adv. 3 (2021) 100054, https://doi.org/10.1016/j. apsadv 2020 100054
- [13] S. Ida, S.J.S. Justin, P. Wilson, B. Neppolian, Facile synthesis of black N-TiO<sub>2</sub> /N-RGO nanocomposite for hydrogen generation and electrochemical applications: new insights into the structure-performance relationship, Appl. Surf. Sci. Adv. 9 (2022) 100249, https://doi.org/10.1016/j.apsadv.2022.100249.
- [14] N. Cheng, S. Stambula, D. Wang, M.N. Banis, J. Liu, A. Riese, B. Xiao, R. Li, T. K. Sham, L.M. Liu, G.A. Botton, X. Sun, Platinum single-atom and cluster catalysis of the hydrogen evolution reaction, Nat. Commun. 7 (2016) 1–9, https://doi.org/10.1038/ncomms13638.
- [15] T. Reier, M. Oezaslan, P. Strasser, Electrocatalytic oxygen evolution reaction (OER) on Ru, Ir, and pt catalysts: a comparative study of nanoparticles and bulk materials, ACS Catal. 2 (2012) 1765–1772, https://doi.org/10.1021/cs3003098.
- [16] M. Retuerto, L. Pascual, J. Torrero, M.A. Salam, Á. Tolosana-Moranchel, D. Gianolio, P. Ferrer, P. Kayser, V. Wilke, S. Stiber, V. Celorrio, M. Mokthar, D. G. Sanchez, A.S. Gago, K.A. Friedrich, M.A. Peña, J.A. Alonso, S. Rojas, Highly active and stable OER electrocatalysts derived from Sr<sub>2</sub>MIrO<sub>6</sub> for proton exchange membrane water electrolyzers, Nat. Commun. 13 (2022), https://doi.org/ 10.1038/ed1467.002.35631.5
- [17] M.A. Lukowski, A.S. Daniel, F. Meng, A. Forticaux, L. Li, S. Jin, Enhanced hydrogen evolution catalysis from chemically exfoliated metallic MoS<sub>2</sub> nanosheets, J. Am. Chem. Soc. 135 (2013) 10274–10277, https://doi.org/10.1021/ja404523s.
- [18] M.S. Faber, R. Dziedzic, M.A. Lukowski, N.S. Kaiser, Q. Ding, S. Jin, High-performance electrocatalysis using metallic cobalt pyrite (CoS<sub>2</sub>) micro- and nanostructures, J. Am. Chem. Soc. 136 (2014) 10053–10061, https://doi.org/10.1021/ja504099w.
- [19] D. Voiry, H. Yamaguchi, J. Li, R. Silva, D.C.B. Alves, T. Fujita, M. Chen, T. Asefa, V. B. Shenoy, G. Eda, M. Chhowalla, Enhanced catalytic activity in strained chemically exfoliated WS 2 nanosheets for hydrogen evolution, Nat. Mater. 12 (2013) 850–855, https://doi.org/10.1038/nmat3700.
- [20] D.R. Cummins, U. Martinez, A. Sherehiy, R. Kappera, A. Martinez-Garcia, R. K. Schulze, J. Jasinski, J. Zhang, R.K. Gupta, J. Lou, M. Chhowalla, G. Sumanasekera, A.D. Mohite, M.K. Sunkara, G. Gupta, Efficient hydrogen evolution in transition metal dichalcogenides via a simple one-step hydrazine reaction, Nat. Commun. 7 (2016), https://doi.org/10.1038/ncomms11857.
- [21] D.Y. Wang, M. Gong, H.L. Chou, C.J. Pan, H.A. Chen, Y. Wu, M.C. Lin, M. Guan, J. Yang, C.W. Chen, Y.L. Wang, B.J. Hwang, C.C. Chen, H. Dai, Highly active and stable hybrid catalyst of cobalt-doped FeS2 nanosheets-carbon nanotubes for hydrogen evolution reaction, J. Am. Chem. Soc. 137 (2015) 1587–1592, https://doi.org/10.1021/ja511572q.
- [22] B. Hinnemann, P.G. Moses, J. Bonde, K.P. Jørgensen, J.H. Nielsen, S. Horch, I. Chorkendorff, J.K. Nørskov, Biomimetic hydrogen evolution: moS2 nanoparticles as catalyst for hydrogen evolution, J. Am. Chem. Soc. 127 (2005) 5308–5309, https://doi.org/10.1021/ja0504690.

- [23] D. Kong, H. Wang, Z. Lu, Y. Cui, CoSe<sub>2</sub> nanoparticles grown on carbon fiber paper: an efficient and stable electrocatalyst for hydrogen evolution reaction, J. Am. Chem. Soc. 136 (2014) 4897–4900, https://doi.org/10.1021/ja501497n.
- [24] S. Deng, Y. Zhong, Y. Zeng, Y. Wang, Z. Yao, F. Yang, S. Lin, X. Wang, X. Lu, X. Xia, J. Tu, Directional construction of vertical nitrogen-doped 1T-2H MoSe<sub>2</sub>/graphene shell/core nanoflake arrays for efficient hydrogen evolution reaction, Adv. Mater. 29 (2017) 1–8, https://doi.org/10.1002/adma.201700748.
- [25] Y. Shi, B. Zhang, Recent advances in transition metal phosphide nanomaterials: synthesis and applications in hydrogen evolution reaction, Chem. Soc. Rev. 45 (2016) 1529–1541, https://doi.org/10.1039/c5cs00434a.
- [26] J. Tian, Q. Liu, A.M. Asiri, X. Sun, Self-supported nanoporous cobalt phosphide nanowire arrays: an efficient 3D hydrogen-evolving cathode over the wide range of pH 0–14, J. Am. Chem. Soc. 136 (2014) 7587–7590, https://doi.org/10.1021/ ia503372r.
- [27] G. Zhang, G. Wang, Y. Liu, H. Liu, J. Qu, J. Li, Highly active and stable catalysts of phytic acid-derivative transition metal phosphides for full water splitting, J. Am. Chem. Soc. 138 (2016) 14686–14693, https://doi.org/10.1021/jacs.6b08491.
- [28] S.S.A. Shah, N.A. Khan, M. Imran, M. Rashid, M.K. Tufail, A. ur Rehman, G. Balkourani, M. Sohail, T. Najam, P. Tsiakaras, Recent advances in transition metal tellurides (TMTs) and phosphides (TMPs) for hydrogen evolution electrocatalysis, Membranes 13 (2023) 1–22, https://doi.org/10.3390/ membranes13010113.
- [29] J. Xie, S. Li, X. Zhang, J. Zhang, R. Wang, H. Zhang, B. Pan, Y. Xie, Atomically-thin molybdenum nitride nanosheets with exposed active surface sites for efficient hydrogen evolution, Chem. Sci. 5 (2014) 4615–4620, https://doi.org/10.1039/ c4sc02019g.
- [30] D. Gao, J. Zhang, T. Wang, W. Xiao, K. Tao, D. Xue, J. Ding, Metallic Ni<sub>3</sub>N nanosheets with exposed active surface sites for efficient hydrogen evolution, J. Mater. Chem. A 4 (2016) 17363–17369, https://doi.org/10.1039/C6TA07883D.
- [31] J. Theerthagiri, S.J. Lee, A.P. Murthy, J. Madhavan, M.Y. Choi, Fundamental aspects and recent advances in transition metal nitrides as electrocatalysts for hydrogen evolution reaction: a review, Curr. Opin. Solid State Mater. Sci. 24 (2020) 100805, https://doi.org/10.1016/j.cossms.2020.100805.
- [32] S. Wang, J. Wang, M. Zhu, X. Bao, B. Xiao, D. Su, H. Li, Y. Wang, Molybdenum-carbide-modified nitrogen-doped carbon vesicle encapsulating nickel nanoparticles: a highly efficient, low-cost catalyst for hydrogen evolution reaction, J. Am. Chem. Soc. 137 (2015) 15753–15759, https://doi.org/10.1021/iacs.5b07924.
- [33] L. Liao, S. Wang, J. Xiao, X. Bian, Y. Zhang, M.D. Scanlon, X. Hu, Y. Tang, B. Liu, H. H. Girault, A nanoporous molybdenum carbide nanowire as an electrocatalyst for hydrogen evolution reaction, Energy Environ. Sci. 7 (2014) 387–392, https://doi.org/10.1039/c3ee42441c.
- [34] X. Yan, L. Tian, M. He, X. Chen, Three-dimensional crystalline/amorphous Co/Co<sub>3</sub>O<sub>4</sub> Core/shell nanosheets as efficient electrocatalysts for the hydrogen evolution reaction, Nano Lett. 15 (2015) 6015–6021, https://doi.org/10.1021/acs.nanolett.5b02205.
- [35] S. Lee, Y.C. Chu, L. Bai, H.M. Chen, X. Hu, Operando identification of a side-on nickel superoxide intermediate and the mechanism of oxygen evolution on nickel oxyhydroxide, Chem. Catal. 3 (2023) 100475, https://doi.org/10.1016/j. checat.2022.11.014.
- [36] X. Zhao, J. Wang, J. Kang, X. Wang, H. Yu, C.F. Du, Ni nanoparticles anchoring on vacuum treated Mo<sub>2</sub>TiC<sub>2</sub>T<sub>x</sub> MXene for enhanced hydrogen evolution activity, Chin. J. Struct. Chem. 42 (2023) 100159, https://doi.org/10.1016/j.cjsc.2023.100159.
- [37] S.J. Lee, J. Theerthagiri, P. Nithyadharseni, P. Arunachalam, D. Balaji, A. Madan Kumar, J. Madhavan, V. Mittal, M.Y. Choi, Heteroatom-doped graphene-based materials for sustainable energy applications: a review, Renew. Sustain. Energy Rev. 143 (2021), https://doi.org/10.1016/j.rser.2021.110849.
- [38] S.S.A. Shah, T. Najam, M.S. Javed, M.M. Rahman, P. Tsiakaras, Novel Mn-/Co-N x moieties captured in N-doped carbon nanotubes for enhanced oxygen reduction activity and stability in acidic and alkaline media, ACS Appl. Mater. Interfaces 13 (2021) 23191–23200. https://doi.org/10.1021/acsami.1c03477.
- (2021) 23191–23200, https://doi.org/10.1021/acsami.1c03477.
   [39] J. Zhang, T. Wang, P. Liu, Z. Liao, S. Liu, X. Zhuang, M. Chen, E. Zschech, X. Feng, Efficient hydrogen production on MoNi<sub>4</sub> electrocatalysts with fast water dissociation kinetics, Nat. Commun. 8 (2017) 1–8, https://doi.org/10.1038/ncomms15437
- [40] J.R. McKone, B.F. Sadtler, C.A. Werlang, N.S. Lewis, H.B. Gray, Ni-Mo nanopowders for efficient electrochemical hydrogen evolution, ACS Catal. 3 (2013) 166–169, https://doi.org/10.1021/cs300691m.
- [41] Y. Yu, S.J. Lee, J. Theerthagiri, Y. Lee, M.Y. Choi, Architecting the AuPt alloys for hydrazine oxidation as an anolyte in fuel cell: comparative analysis of hydrazine splitting and water splitting for energy-saving H<sub>2</sub> generation, Appl. Catal. B Environ. 316 (2022) 121603, https://doi.org/10.1016/j.apcatb.2022.121603.
- [42] Y. Yu, S.J. Lee, J. Theerthagiri, S. Fonseca, L.M.C. Pinto, G. Maia, M.Y. Choi, Reconciling of experimental and theoretical insights on the electroactive behavior of C/Ni nanoparticles with AuPt alloys for hydrogen evolution efficiency and Nonenzymatic sensor, Chem. Eng. J. 435 (2022) 134790, https://doi.org/10.1016/j. cej.2022.134790.
- [43] S. Mo, H. Zhong, F. Liu, Y. Tang, S.S.A. Shah, S.J. Bao, A salt-baking 'recipe' of commercial nickel-molybdenum alloy foam for oxygen evolution catalysis in water splitting, J. Colloid Interface Sci. 640 (2023) 975–982, https://doi.org/10.1016/j. icis. 2023.02.114
- [44] K. Wang, J. Wu, S. Zheng, S. Yin, NiCo alloy nanoparticles anchored on mesoporous Mo<sub>2</sub>N nanosheets as efficient catalysts for 5-hydroxymethylfurfural electrooxidation and hydrogen generation, Chin. J. Struct. Chem. 42 (2023) 100104, https://doi.org/10.1016/j.cjsc.2023.100104.

- [45] M. Li, L. Feng, NiSe<sub>2</sub>-CoSe<sub>2</sub> with a hybrid nanorods and nanoparticles structure for efficient oxygen evolution reaction, Chin. J. Struct. Chem. 1 (2022) 19–24, https:// doi.org/10.14102/j.cnki.0254-5861.2021-0037.
- [46] J. Zhang, C. Zhang, X. Duo, Z. Liu, C. Liu, L. Guo, A. Xie, S. Luo, Self-assembled acicular CuCo-MOF for enhancing oxygen evolution reaction, Ionics 26 (2020) 5123–5132, https://doi.org/10.1007/s11581-020-03651-0 (Kiel).
- [47] S. Naik Shreyanka, J. Theerthagiri, S.J. Lee, Y. Yu, M.Y. Choi, Multiscale design of 3D metal-organic frameworks (M-BTC, M: cu, Co, Ni) via PLAL enabling bifunctional electrocatalysts for robust overall water splitting, Chem. Eng. J. 446 (2022) 137045, https://doi.org/10.1016/j.cej.2022.137045.
- [48] S.S.A. Shah, T. Najam, M.K. Aslam, M. Ashfaq, M.M. Rahman, K. Wang, P. Tsiakaras, S. Song, Y. Wang, Recent advances on oxygen reduction electrocatalysis: correlating the characteristic properties of metal organic frameworks and the derived nanomaterials, Appl. Catal. B Environ. 268 (2020) 118570, https://doi.org/10.1016/j.apcatb.2019.118570.
- [49] T. Najam, S.S.A. Shah, W. Ding, Z. Wei, Role of p-doping in antipoisoning: efficient mof-derived 3d hierarchical architectures for the oxygen reduction reaction, J. Phys. Chem. C 123 (2019) 16796–16803, https://doi.org/10.1021/acs. jpcc.9b03730.
- [50] D.H. Taffa, D. Balkenhohl, M. Amiri, M. Wark, Minireview: ni–Fe and Ni–Co metal–organic frameworks for electrocatalytic water-splitting reactions, Small. Struct. 4 (2023) 1–21, https://doi.org/10.1002/sstr.202200263.
- [51] B. Zhang, Y. Zheng, T. Ma, C. Yang, Y. Peng, Z. Zhou, M. Zhou, S. Li, Y. Wang, C. Cheng, Designing MOF nanoarchitectures for electrochemical water splitting, Adv. Mater. 33 (2021) e2006042, https://doi.org/10.1002/adma.202006042.
- [52] X. Xing, Y. Song, W. Jiang, X. Zhang, CuFe–P from a Prussian blue analogue as an electrocatalyst for efficient full water splitting, Sustain. Energy Fuels 4 (2020) 3985–3991, https://doi.org/10.1039/D0SE00402B.
- [53] R. Nivetha, A. Sajeev, A. Mary Paul, K. Gothandapani, S. Gnanasekar, G. Jacob, R. Sellappan, V. Raghavan, N. Krishna Chandar, S. Pitchaimuthu, S.K. Jeong, A. Nirmala Grace, Cu based metal organic framework (Cu-MOF) for electrocatalytic hydrogen evolution reaction, Mater. Res. Express. 7 (2020), https://doi.org/10.1088/2053-1591/abb056.
- [54] Q. Liu, J. Chen, F. Yu, J. Wu, Z. Liu, B. Peng, Multifunctional book-like CuCo-MOF for highly sensitive glucose detection and electrocatalytic oxygen evolution, New J. Chem. 45 (2021) 16714–16721, https://doi.org/10.1039/dlinj02931b.
- [55] A. Macedo Andrade, Z. Liu, S. Grewal, A.J. Nelson, Z. Nasef, G. Diaz, M.H. Lee, MOF-derived Co/Cu-embedded N-doped carbon for trifunctional ORR/OER/HER catalysis in alkaline media, Dalton Trans. 50 (2021) 5473–5482, https://doi.org/ 10.1039/D0DT04000B.
- [56] Y. Zhou, B. Tang, S. Wang, J. Long, Cu-MOF@Co-MOF derived Co-Cu alloy nanoparticles and N atoms co-doped carbon matrix as efficient catalyst for enhanced oxygen reduction, Int. J. Hydrog. Energy 45 (2020) 15785–15795, https://doi.org/10.1016/ji.jipydene.2020.04.049.
- [57] S.S.A. Shah, T. Najam, C. Cheng, L. Peng, R. Xiang, L. Zhang, J. Deng, W. Ding, Z. Wei, Exploring Fe-Nx for peroxide reduction: template-free synthesis of Fe-Nx traumatized mesoporous carbon nanotubes as an ORR catalyst in acidic and alkaline solutions, Chem. A Eur. J. 24 (2018) 10630–10635, https://doi.org/10.1002/chem.201802453.
- [58] J. Theerthagiri, K. Karuppasamy, S.J. Lee, R. Shwetharani, H.S. Kim, S.K.K. Pasha, M. Ashokkumar, M.Y. Choi, Fundamentals and comprehensive insights on pulsed laser synthesis of advanced materials for diverse photo- and electrocatalytic applications, Light Sci. Appl. 11 (2022), https://doi.org/10.1038/s41377-022-00904-7.
- [59] Y. Yu, J. Theerthagiri, S.J. Lee, G. Muthusamy, M. Ashokkumar, M.Y. Choi, Integrated technique of pulsed laser irradiation and sonochemical processes for the production of highly surface-active NiPd spheres, Chem. Eng. J. 411 (2021) 128486, https://doi.org/10.1016/j.cej.2021.128486.
- [60] M. Zhong, S. Zhang, A. Dong, Z. Sui, L. Feng, Q. Chen, Cu-MOF/Au–Pd composite catalyst: preparation and catalytic performance evaluation, J. Mater. Sci. 55 (2020) 10388–10398, https://doi.org/10.1007/s10853-020-04699-z.
- [61] D. Jiang, T. Mallat, D.M. Meier, A. Urakawa, A. Baiker, Copper metal-organic framework: structure and activity in the allylic oxidation of cyclohexene with molecular oxygen, J. Catal. 270 (2010) 26–33, https://doi.org/10.1016/j. icat/2009.12.002
- [62] M.G. Radhika, B. Gopalakrishna, K. Chaitra, L.K.G. Bhatta, K. Venkatesh, M. K. Sudha Kamath, N. Kathyayini, Electrochemical studies on Ni, Co & Ni/Co-MOFs for high-performance hybrid supercapacitors, Mater. Res. Express. 7 (2020), https://doi.org/10.1088/2053-1591/ab8d5d.
- [63] J. Long, K. Shen, L. Chen, Y. Li, Multimetal-MOF-derived transition metal alloy NPs embedded in an N-doped carbon matrix: highly active catalysts for hydrogenation reactions, J. Mater. Chem. A 4 (2016) 10254–10262, https://doi.org/10.1039/ c6ta00157b.
- [64] Nagajyothi, CuO and Co $_3$ O $_4$  nanoparticles: synthesis, characterizations, and Raman spectroscopy, < 2013 (2013) 926–931, https://doi.org/10.1155/2013/714853.
- [65] M. Wang, J. Huang, M. Wang, D. Zhang, W. Zhang, W. Li, J. Chen, Co<sub>3</sub>O<sub>4</sub> nanorods decorated reduced graphene oxide composite for oxygen reduction reaction in alkaline electrolyte, Electrochem. Commun. 34 (2013) 299–303, https://doi.org/ 10.1016/j.elecom.2013.07.017.
- [66] Z. Neisi, Z. Ansari-Asl, A.S. Dezfuli, Polyaniline/Cu(II) metal-organic frameworks composite for high performance supercapacitor electrode, J. Inorg. Organomet. Polym. Mater. 29 (2019) 1838–1847, https://doi.org/10.1007/s10904-019-01145 0
- [67] F.T. Alshorifi, S.M. El Dafrawy, A.I. Ahmed, Fe/Co-MOF nanocatalysts: greener chemistry approach for the removal of toxic metals and catalytic applications, ACS Omega 7 (2022) 23421–23444, https://doi.org/10.1021/acsomega.2c01770.

- [68] N. Alizadeh, A. Salimi, T.K. Sham, CuO/Cu-MOF nanocomposite for highly sensitive detection of nitric oxide released from living cells using an electrochemical microfluidic device, Microchimica Acta 188 (2021) 1–11, https://doi.org/10.1007/s00604-021-04891-1.
- doi.org/10.1007/s00604-021-04891-1.
   [69] M. Zhong, D.H. Yang, L.J. Kong, W. Shuang, Y.H. Zhang, X.H. Bu, Bimetallic metalorganic framework derived Co<sub>3</sub>O<sub>4</sub>-CoFe<sub>2</sub>O<sub>4</sub> composites with different Fe/Co molar
- ratios as anode materials for lithium ion batteries, Dalton Trans. 46 (2017) 15947–15953, https://doi.org/10.1039/c7dt03047a.
- [70] M. Tou, R. Michalsky, A. Steinfeld, Solar-driven thermochemical splitting of CO<sub>2</sub> and in situ separation of CO and O<sub>2</sub> across a ceria redox membrane reactor, Joule 1 (2017) 146–154, https://doi.org/10.1016/j.joule.2017.07.015.